A novel combination of cyclophosphamide and anti-ICOS mAb prevents tumor growth by affecting regulatory T cells in mice with a human immune system

Aude Burlion [1], Rodrigo N. Ramos [2,3], Kélhia Sendeyo [1], Aurélien Corneau [4], Christine Ménétrier-Caux [5,6], Eliane Piaggio [2,3], Daniel Olive [7], Christophe Caux [5,6] and Gilles Marodon [1*]

1 Sorbonne Université, CNRS, INSERM U1135, Centre d'Immunologie et des Maladies Infectieuses (CIMI), 75013 Paris, France.

2 Institut Curie, PSL Research University, INSERM U932, 75005 Paris, France.

3 SiRIC Translational Immunotherapy Team, Translational Research Department, Research Center, PSL Research University, Institut Curie, 75005 Paris, France.

4 Sorbonne Université, UMS 30, Plateforme de Cytométrie, 75013 Paris, France.

5 INSERM 1052, CNRS 5286, Centre Léon Bérard, Centre de Recherche en Cancérologie de Lyon, Univ Lyon, Université Claude Bernard Lyon 1, Lyon, France.

6 Department of Translational Research and Innovation, Centre Léon Bérard, Lyon, France.

7 Centre de recherche en Cancérologie de Marseille, INSERM U1068, CNRS, Aix Marseille Université, Institut Paoli - Calmettes, Marseille, France.

* To whom correspondence should be addressed: gilles.marodon@upmc.fr

Abstract

Mice reconstituted with a human immune system and bearing human tumors represent a promising model for developing novel cancer immunotherapy strategies. However, the nature of tumor infiltrating leukocytes in humanized mice and whether they can be mobilized to control tumor growth is currently unknown. Here, we used mass cytometry and multi parametric flow cytometry to characterize human leukocytes infiltrating a human breast cancer tumor model in CD34-reconstituted NOD.SCID.γc-null mice and compared it to breast cancer patient's samples. We unambiguously detected human T cells, monocytes and plasmacytoid dendritic cells in the tumors of humanized mice. Importantly, activated/memory T cells and $ICOS^+$ regulatory T cells were enriched in the tumor relative to the periphery both in humanized mice and in breast cancer patients. The presence of $ICOS^+$ regulatory T cells in the tumor has been associated with poor survival in breast cancer patients. Administration of a neutralizing mAb to human ICOS reduced regulatory T cells, and a combination of the anti-ICOS mAb and chemotherapy reduced tumor growth whereas single treatments had no or little effects. Besides characterizing human leukocytes in tumors of humanized mice, we show that a combination of anti-ICOS and chemotherapy can mobilize human leukocytes to control tumor growth *in vivo*, making it a promising strategy in humans.

Introduction

Preventing immune suppression in tumors is the "next frontier" in immuno-oncology research. Despite recent success of anti-PD-1 mAbs for metastatic melanomas and other types of malignancies, it seems reasonable to propose that combination therapy will be key to the success of future cancer immunotherapy strategies, as suggested in patients receiving a combination of anti-PD-1 and anti-CTLA-4 *(1)*. Likely, the most efficient combinations would emerge from the vast list of mechanisms that prevent an efficient immune response *(2)*. Recently, a murine study combining a tumor-targeting mAb, a recombinant cytokine, an anti-PD-1 mAb and a T cell vaccine achieved a remarkable efficacy at clearing large established tumors *(3)*, illustrating the power of combinations for T-cell and innate cell mediated tumor control. However, studies purely performed in murine models are only useful to gain biological insights but are no more relevant to validate mAbs or drugs targeting selectively human cells. Clinical data will be invaluable to decide which combinations work best on a defined set of cancers but clinical trials in patients are costly and lengthy. Moreover, it will not be possible to test every combination of treatments in large-scale clinical trials, raising the possibility that some efficient combinations might be missed. Therefore, a mouse model in which combination therapies targeting human cells could be tested would be most invaluable.

It has been shown that human breast tumor morphology and metastatic properties were conserved in xenograft immunodeficient mice *(4, 5)*. This was also showed for ovarian cancers *(6)* and latter confirmed for melanomas *(7)*, suggesting that a large panel of human tumors engrafts efficiently in immunodeficient mice and reproduces features of clinical progression. Xenograft models might be useful to target human tumors but these immunodeficient models are not relevant to test drugs such as mAbs that target the human immune system. Mice carrying a human immune system (HuMice) and human tumors could therefore represent the "ideal" model for cancer immunotherapy research, at the interface of mice and humans *(8)*. Most of the literature regarding the use of HuMice for immuno-oncology relies on direct transfer of total PBMC into immunodeficient mice of various genetic backgrounds. Therapeutic efficacy of a combination of an anti-PD-1 and an anti-4-1-BB mAbs has been demonstrated in a model in which the tumor and the PBMC were from the same patient, highlighting the unique feature of this model for cancer immunotherapy studies in an autologous setting *(9)*. However, PBMC-implanted mice invariably and rapidly suffer from Graft vs Host Disease, which complicate the interpretation of the results and limits the duration of the experiments. To preclude this

problem, NOD.SCID.gamma-c-null (NSG) immunodeficient mice can be reconstituted with human hematopoietic progenitors *(10)*, most often isolated from allogeneic cord blood $CD34^+$ cells. Because we demonstrated that a pool of human T cells with a diverse repertoire was then generated *(11)*, it becomes feasible to assess combination therapy targeting the tumor and/or T cells, with meaningful results potentially transposable to the clinic. However, there is still a lack of information on the composition and the function of human leukocytes infiltrating human tumors in HuMice. Indeed, very few studies have evaluated the nature of human leukocytes in CD34-reconstituted HuMice *(12–16)*. Activated T cells in the tumor were observed in a peculiar model of tumor implantation at birth in NSG mice that did not lead to tumor rejection *(12)*. A more advanced model of HuMice (MISTRG) was used to decipher the contribution of the innate immune system to tumor control, but the presence of T cells in the tumor was not reported *(14)*. Very few T cells were detected in a Patient-Derived Xenograft (PDX) model of head and neck squamous cell carcinomas *(15)*. Likewise, very few T cells were detected in breast cancer-bearing NSG mice with myeloid cells being the subset the most represented in the tumor *(13)*. Finally, a recent study described the presence of $CD4^+$ regulatory T cells (Treg) in the tumor of NSG mice but a precise quantification of T cells was not reported *(16)*. Thus, the presence of human T cells in tumors of HuMice is still open to debate. This is a crucial question to be answered if one wants to use the model in a reliable and relevant way.

Without tumors, the expected effects of the mAbs Teplizumab (anti-CD3) and Ipilimumab (anti-CTLA-4) , were successfully reproduced in CD34-HuMice *(17, 18)* , and Avastin (anti-VEGF) had the expected effect on tumor growth *(14)*, showing that human-specific mAbs are effective in HuMice. A recent study found that a humanized IgG1 mAb targeting the TNFR family member GITR, currently in clinical trial, was effective at preventing growth of a melanoma cell line in NSG HuMice *(16)*. Thus, novel mAbs that would be effective on tumor control in HuMice might represent promising candidates for cancer immunotherapy in humans.

Cytometry Time-of-flight (CyTOF) or mass cytometry is a recent technology allowing quantification of the expression of 30 to 40 proteins at the same time at the single cell level *(19)*, a very useful feature when analyzing samples containing a limited number of cells. Here, we used a combination of single-cell mass cytometry and high dimension flow cytometry to compare the immune landscape of human breast cancer in CD34-reconstituted NSG and in patients, as a reference. From this analysis, the Inducible COStimulatory molecule (ICOS) emerged in both human and HuMice as an eligible marker to target Treg, a crucial T cell subset dampening the anti-tumoral immune response

(20). We provide the first proof-of-principle that a combination of chemotherapy and anti-ICOS mAb affected Treg and reduced tumor growth in HuMice, opening the possibility to translate this combination into the clinics.

Results

T cell infiltrate in the tumors of HuMice

The experimental design of our study is represented on Fig. 1A. Irradiated NSG newborns were injected in the liver with cord blood $CD34^+$ cells. Sixteen to 20 weeks after, mice were grafted s.c with MDA-MB-231 human breast cancer cells. After 30 to 40 days, mice were euthanized and the spleen and tumors were analyzed by mass cytometry. The CyTOF panel was designed to include the most common lineage markers for murine and human leukocytes, but also several activation and proliferation markers of human T lymphocytes (Table S1). To normalize the variability between mice for supervised (i.e 2D plots) and unsupervised (i.e tSNE) analysis, samples from tumors and spleen individually acquired on the CyTOF were pooled by concatenation.

We first compared the frequencies of human and murine cells of the hematopoietic lineage ($CD45^+$) in the spleen and in the tumor in 4 independent experiments, totalizing 15 CD34-reconstituted NSG mice. In the spleen, human $CD45^+$ cells represented 30% of all cells on average whereas murine cells represented only 10% (Fig. 1B). Frequencies of human and murine $CD45^+$ cells were much lower in the tumor, representing 1% of all cells on average (Fig. 1C). Thus, the leukocyte content of the tumor in HuMice was a mix of human and murine hematopoietic cells. Within human cells, a classical 2D analysis of the CyTOF data revealed the presence of $CD3^+$, $CD20^+$ B cells, $CD4^+$ and $CD8^+$ T cells in the spleen and the tumor (Fig. 1D). To gain deeper insights on the nature of immune cells present in the tumor environment, we performed unsupervised clustering of the data using the tSNE algorithm. This algorithm reduces the multidimensional nature of mass cytometry data to a 2D representation (viSNE), in which each dot is a cell, clustered according to level of expression of chosen markers *(21)*. We first focused our analysis on manually gated $hCD45^+$ and ran the tSNE algorithm based on lineage and activation markers. Clusters of $CD20^+$, $CD3^+$, $CD4^+$ and $CD8^+$ cells were readily detected in the spleen and tumor with that method. Some minor clusters of $CD3^{neg}$ cells that did not express CD4 nor CD8 were also revealed (Fig. 1E). $CD20^+$ B cells were almost absent from the tumor in 3/3 experiments in which B cells were detected in the spleen. In contrast, there was no major differences in the frequencies of $CD3^+$, $CD4^+$ cells and $CD8^+$ T cells in the tumor and in the spleen of HuMice (Fig. 1F). Thus, these results unequivocally demonstrate that human tumors of HuMice are infiltrated by

human T cells, a *sine qua non* condition for the usefulness of the model for cancer immunotherapy research.

Innate immune cells in the tumors of HuMice

Notably, a distinct cluster of non-T non-B myeloid CD33$^+$ HLA-DR$^+$ cells was observed in the spleen and tumor of HuMice (Fig. 2A). Zooming on in CD33$^+$, two distinct populations of CD14$^+$HLA-DR^{lo} and CD123$^+$HLA-DR^{hi} cells further segregate, showing that these were different subsets, most likely representing monocytes and plasmacytoid dendritic cells (pDCs) precursors, since pDC precursors and pDCs might differ by CD33 expression (22) (Fig. 2B). A subset of CD33$^+$ cells did not express CD14 nor CD123, were heterogeneous for HLA-DR and were enriched in the tumor, likely including classical DC. In addition, two clusters of Granzyme-B-expressing cells (Grz-B$^+$) were observed in the spleen and the tumor (Fig. 2C): one expressed CD8 (Fig. 1E) and thus represented CTL, while the others expressed CD335 (NKp46) cells and thus represented NK cells. In this later cluster, NKp46 expression was lower in the tumor than in the spleen. Thus, in addition to CD4$^+$ and CD8$^+$ T cells, which represented the vast majority of human cells, the immune landscape of tumors in CD34-HuMice also included monocytes, pDC and NK cells.

The same unsupervised representation of the data was performed on gated mCD45$^+$ cells based on myeloid-specific lineage markers (Fig. S1A). As expected from lymphoid-deprived NSG mice, most mCD45$^+$ cells expressed CD11b in the spleen and the tumor (Fig. S1B). Clusters of Ly-6C$^+$ monocytes, Ly6-G$^+$ neutrophils and CD11c$^+$ DC were readily observed in the spleen and the tumor (Fig. S1B). Overall, myeloid cells of NSG mice were similarly represented in the spleen and the tumor, with the exception of Ly6G$^+$ neutrophils which were less abundant in the tumor (Fig. S1C).

The tumor immune landscape in breast cancer patients

To compare the distribution of human leukocytes in HuMice to human samples, we determined the distribution of human leukocytes in the blood and tumors of 7 breast cancer patients by 17-color flow cytometry. On a representative patient, the t-SNE algorithm efficiently isolated CD19$^+$, CD3$^+$, CD4$^+$ and CD8$^+$ T cells, as well as CD4^{lo}CD14$^+$ monocytes in the blood and the tumor (Fig. 3A). There was a lower proportion of B cells and CD14$^+$ cells in the tumor than in the blood (Fig. 3B). In contrast,

there was a higher frequency of $CD3^+$ T cells in the tumor, mostly due to an increase in $CD8^+$ T cells (Fig. 3B). Collectively, NSG humanized mice model recapitulates key characteristics found in human tumors from patients, notably lower frequencies of B cells and $CD14^+$ monocytes and higher frequencies of $CD3^+$ T cells (from 60 to 80% of all $hCD45^+$ cells) in the tumor relative to the periphery.

Highly activated Tumor-infiltrating T cells in HuMice and breast cancer patients

Having established unambiguously that tumors in HuMice contained human T cells, we next investigated the activation status of those human T cells. We performed a t-SNE analysis on human $CD3^+$ T cells, allowing visualization of two main clusters of $CD4^+$ and $CD8^+$ T cells (Fig. 4A). When activation and functional markers such as CD45RO, HLA-DR, PD-1, CD25 or Grz-B were considered, we noticed a general increase in high expressing cells in the tumor relative to the spleen for both $CD4^+$ and $CD8^+$ cells, a first indication that T cells were activated in the tumor. Up regulation of CD45RO and HLA-DR expression was observed in both $CD4^+$ and $CD8^+$ subsets whereas higher PD-1 and CD25 expression was noted among $CD4^+$ T cells. As expected, up regulation of Grz-B expression was restricted to $CD8^+$ T cells. These main features were reproduced across 3 independent experiments (Fig. S2). To determine the activation status of human T cells more precisely, we performed a boolean analysis calculating the frequencies of cells expressing 0, 1, any combination of 2 or all 3 above mentioned activation markers in $CD4^+$ and $CD8^+$ T cells. Results depicted in Fig. 4B show that the frequencies of $CD4^+$ or $CD8^+$ cells co expressing 2 or 3 activation markers were vastly increased in the tumor, while frequencies of T cells expressing none of the activation markers were drastically reduced. Despite this massive activation, the frequencies of proliferating $Ki\text{-}67^+$ cells co-expressing 3 activation markers were lower in tumors relative to the spleen, although it did not reach statistical significance by multiple comparisons probably owing to a lack of statistical power (Fig. S3A). Of note, PD-1 expression was correlated with higher proliferation of $CD4^+$ and $CD8^+$ T cells in the spleen whereas it was inversely correlated with proliferation in $CD4^+$ but not $CD8^+$ T cells in the tumor (Fig S3B-D), suggesting that PD-1 expression might explain the hypoproliferative status of $CD4^+$ but not $CD8^+$ T cells in the tumor. Importantly, a similar enrichment for activated/memory T cells was observed in the tumor relative to the blood in breast cancer patients, assessed by the co expression of 2 or 3 activation markers (Fig. 4C). Thus, tumor infiltrating T cells were highly activated in both HuMice and breast cancer patients.

Increased expression of ICOS on regulatory T cells of breast cancer patients and HuMice

Effector Treg are defined by the expression of the transcription factor FOXP3 and the IL-2R-alpha chain CD25, and by the lack of CD45RA expression *(23)*. They are important actors of immunosuppression in the tumors of human patients. It has also been shown that ICOS /ICOSL interaction can regulate Treg functions in humans *(24)* and observations from authors of the present study linked ICOS expression to Treg-mediated immunosuppression in breast cancer patients *(25, 26)*. Furthermore, authors of the present study reported a correlation between ICOS expression and poor prognosis in breast cancer patients due to its promoting action on Treg *(26, 27)*. A distinct cluster of $CD4^+$ cells expressing FOXP3, high levels of ICOS and negative for CD45RA, thus of an effector Treg phenotype, were detected at higher frequencies in tumors of breast cancer patients compared to blood (Fig. 5A-B). It has been shown in humans that $CD4^+FOXP3^+CD45RA^{neg}$ cells might include activated effector T cells with lower FOXP3 expression than effector Treg *(23)*. We observed that the frequencies of $ICOS^+$ cells were higher in $FOXP3^{hi}$ cells than in $FOXP3^{lo}$ cells in the tumor (Fig. 5C), suggesting that $CD4^+CD45RA^{neg}FOXP3^{hi}ICOS^+$ cells represented *bona fide* effector Treg. The higher expression of ICOS on Treg of the tumor was also documented by an increase in the MFI of ICOS in $FOXP3^+$ vs. $FOXP3^{neg}$ cells (Fig. 5D). Importantly, a similar increase was observed in the tumors of HuMice (Fig. 5E), showing that over expression of ICOS by Treg in human tumors was recapitulated in HuMice. We thus surmise that ICOS could represent a suitable target to affect Treg, with a possible impact on tumor growth, a testable hypothesis in HuMice.

Combination of chemotherapy and anti-ICOS to control tumor growth in HuMice

To test the hypothesis that ICOS/ICOS-L neutralization might affect Treg *in vivo*, we injected once an anti-hICOS antagonist mAb *(26)* in HuMice and determined the frequencies of Treg in the spleen and the tumor 30 days after. Technical issues prevented CyTOF analysis of these experiments. Thus, regular flow cytometry was performed to determine frequencies of $FOXP3^+ICOS^+$ and $FOXP3^+CD25^+$ cells following treatment. There was a statistically significant effect of the treatment on the proportions of $FOXP3^+ICOS^+$ cells ($p=0.0027$, 2-way ANOVA) and of $FOXP3^+CD25^+$ cells ($p=0.0039$, 2-way ANOVA) in the spleen and the tumor combined. By multiple comparisons with

corrected p-values, the treatment led to a statistically significant reduction in the frequencies of FOXP3$^+$ cells expressing CD25 or ICOS in the spleen of HuMice and similar tendencies were observed in the tumor (Fig. 6A). The treatment also affected the absolute numbers of total T cells in the spleen, roughly by a factor of 6, but that did not reach statistical significance. In contrast, Treg counts were significantly reduced by the treatment with numbers dropping almost 20-fold (Fig. 6B). Moreover, the anti-ICOS mAb treatment was associated with increased proliferation of FOXP3+CD25+, total CD4+ but not CD8+ T cells in the spleen (Fig S4). Thus, the anti-ICOS mAb led to a significant reduction of FOXP3$^+$ cells in treated animals and also improved proliferation of CD4$^+$ T cells.

To evaluate the impact of the mAb on tumor growth, HuMice with similar T cell reconstitution prior the initiation of the experiments (Fig. S5) were entered into a pre-clinical-like trial with random assignments into groups, blinded evaluation, mixed sex ratio and sufficient number of animals to detect the observed effect with enough statistical power. The anti-ICOS mAb injected alone had no effect on tumor growth, showing that the reduction in Treg that we report above was not sufficient to significantly impact tumor growth (Fig. 6C). It was recently shown in syngeneic murine models that combining immunotherapy with chemotherapy can be more efficient than each treatment alone *(28)*. Cyclophosphamide (CTX) is widely used as a chemotherapy for treatment of breast cancer and has been described as a potent inducer of immunogenic cell death (ICD) *(29)*. Anti-ICOS mAb combined with CTX at a dose of 1.5 mg that only moderately affected tumor growth in non-humanized NSG mice (Fig S6) and HuMice (Fig. 6C) in order for the combination effect to be seen, profoundly reduced tumor growth in HuMice compared to single treatments (Fig. 6C). Moreover, only mice from the combination group presented very small tumors at the end of the experiment, a sign of efficient control of tumor growth (Fig. 6D). Thus, a combination of CTX with neutralizing anti-ICOS mAb efficiently controlled tumor growth in CD34-reconstituted HuMice.

Role of human T cells in the control of tumor growth by the combination of chemotherapy and anti-ICOS mAb

Lower rather than higher frequencies of human CD45$^+$CD3$^+$ cells were observed in the tumor of the combo group relative to the other groups, indicating that tumor control was not associated to increased tumor infiltration by human T cells (Fig. 7A). To further investigate the role of human T cells, we injected HuMice with a chimeric CD8-depleting recombinant Ig *(30)* after tumor implantation

and before the combination of treatments. As observed in our previous work in CD34-reconstituted HuMice *(31)*, efficient $CD8^+$ T cell depletion was observed in the spleen and tumors of euthanized animals and was reflected by a large increase in the CD4 to CD8 ratio (Fig. S7). However, tumor growth in the combo group was unaffected by the absence of $CD8^+$ T cells, showing that these could not be solely responsible for better tumor control (Fig. 7B).

To assess whether a distinct cytokine profile could be associated to treatment efficacy, we evaluated *ex vivo* frequencies of splenocytes positive for IL-2, TNFα and IFNγ in $CD4^+$ and $CD8^+$ T cells in the various groups upon polyclonal stimulation. A boolean analysis was used to determine frequencies of all 7 possible subsets. Among those 7 subsets, only 4 were represented at frequencies above 1% and are represented in Fig. 7C. Overall, there was no effect of the treatment on frequencies of cytokine-expressing cells in $CD8^+$ T cells ($p=0.63$ by 2-way ANOVA), in agreement with the hypothesis that those play no or little role in tumor control. In contrast, frequencies of cytokine-expressing $CD4^+$ T cells were affected by the treatment ($p=0.039$ by 2-way ANOVA). Notably, there was a reduction in the proportion of $CD4^+$ cells expressing IL-2 (with and without TNFα), and a tendency for higher IFNγ production in the combo group relative to the control group. Thus, tumor control in the combo group was correlated to a reduction in the frequencies of $IL\text{-}2^+$ $CD4^+$ T cells in the spleen which was somehow compensated for by an increase in $IFN\gamma^+$ cells.

Discussion

In the present study, we provide the first demonstration that CD34-reconstituted HuMice can be used as a platform for the discovery and the validation of novel combinations of chemotherapy and immunotherapy, potentially applicable to patients. This demonstration originates from several similarities between HuMice and patients that we reveal here using multiparametric flow and mass cytometry. A first similarity that we uncover here is the composition of the tumor immune landscape. Within total human hematopoietic cells, it is remarkable to note that a similar proportion of $CD3^+$ T cells infiltrated the tumors in patients and in HuMice. We also observed similar infiltration of memory/activated $CD4^+$ and $CD8^+$ T cells that expressed a combination of activation markers. However, this activation status did not translate into increased proliferation in the tumor of HuMice, suggesting that the tumor microenvironment of this triple negative (TN) $PR^{neg}ER^{neg}HER\text{-}2^{neg}$ cell line might be immunosuppressive *in vivo*. The immunosuppressive status of the tumor microenvironment in breast cancer patients is still unclear and might depend on the nature of the tumor, that is estrogen-dependency and/or HER2/Neu expression, that may condition T cell infiltrate and T cell activation status *(32)*. It is remarkable to note that TN-bearing cancer presents the highest T cell infiltrate (33), $CD8^+$ and $FOXP3^+$ T cells alike, opening the possibility that TN breast cancer might be an immunosuppressive-prone microenvironment. Thus, by several accounts, the immune landscape of HuMice bears several similarities with breast cancer patients. Perhaps the most striking similarity that we described here is the enrichment for ICOS-expressing Treg in patients and in HuMice, in agreement with our previously published results describing the presence of $ICOS^+$ Treg in the breast cancer micro-environment *(25)*. The pDC subset that we describe here for the first time in the tumor of HuMice might have played a role on the amplification of ICOS+ Treg, as described in patients *(26)*. The similarity of the Treg phenotype in tumors of patients and HuMice based on ICOS expression opened the possibility to intervene with an anti-ICOS mAb to affect Treg, with possible impact on tumor growth.

The CD28-superfamily belonging ICOS is an essential co stimulatory molecule for T cell activation and function *(35, 36)*. Although originally thought of as a co stimulatory molecule for effective T helper cell response *(37)*, the biology of ICOS now extends well beyond this restricted view *(38)*. Relevant to the present study, we and others have shown that the survival, the expansion, and the suppressive functions of human Treg were dependent on ICOS signaling *(24, 26, 39)*. Thus, one

possibility to explain higher expression of ICOS on human Treg is that a constant signaling through ICOS would be needed to maintain proper Treg homeostasis. The reduction in the absolute numbers of Treg after anti-ICOS mAb treatment that we report here is in line with that hypothesis. We cannot exclude that physical depletion of Treg by the mAb, as observed for $CD8^+$ T cells with the chimeric anti-CD8 recombinant Ig, might also have played a role. The murine nature of the IgG1 anti-ICOS mAb used herein might have engaged FcRs expressed by myeloid cells, leading to active deletion of ICOS-expressing cells. Although a similar mechanism has been proposed to explain anti-tumoral effect and Treg depletion following administration of a murine IgG2a isotype to GITR in mice *(40)*, murine IgG1 isotype is not recognized as a potent inducer of ADCC. As put forward in the study of Bulliard et al *(40)*, much remains to be done to decipher the mechanisms responsible for mAb-mediated T cell depletion in mice. Of note, Treg depletion is now considered a major mechanism for therapeutic efficacy of anti-CTLA-4 or anti-OX40 mAbs in mice *(41–43)* and possibly of Ipilimumab in humans *(44)*. Several mAbs targeting Treg are in development or already approved, including but not limited to anti-CCR4 *(45)*, anti-OX-40 *(46)* and anti-GITR mAb (47). In addition, the chemokine receptor CCR8 was recently proposed as an attractive target to affect Treg in breast cancer and alleviate immunosuppression, although this was not directly demonstrated *(48)*. Our results indicate that ICOS might be a useful addition to this growing list of Treg-specific targets.

In line with published results in murine models *(49)*, we confirm here that blocking ICOS alone was not sufficient to impact tumor growth, despite Treg depletion. However, a combination of chemotherapy and anti-ICOS mAb significantly impacted tumor growth in CD34-HuMice. This result support a role for Treg depletion in the context of ICD of the tumor, and strongly suggest that proper activation of effector T cells in the absence of Treg is necessary to control tumor growth in HuMice. Indeed, we were able for the first time in HuMice to investigate directly the role of human $CD8^+$ T cells in tumor control. Surprisingly, the results do not support an important role for $CD8^+$ T cells on tumor control in the combination group, and this is further supported by their unaltered cytokine expression profile detected *ex vivo*. Rather, we surmise that $CD4^+$ T cells, by their improved capacity to produce IFN-γ and their reduced production of the pro-Treg cytokines IL-2 and TNF-α, at least in the spleen, might be central for tumor control following the combined treatment. Multiple mechanisms of action for $CD4^+$ T cells are possible and remains to be investigated. It is also not clear if the improvement in $CD4^+$ T cells poly-functionality is a consequence of the reduction in Treg or results from a direct action of the antibody on effector cell activation. In addition to human $CD3^+$ T cells, the tumors of HuMice

also contained rare populations of immune cells known to play important roles on the anti-tumor immune response, such as monocytes or DCs. It will be important in the future to monitor the myeloid compartment more closely, since those cells can positively *(50)* and/or negatively affect the local anti-tumor immune response *(51)*. We also reveal the presence of NK cells with low expression of NKp46 in the tumor, suggesting impaired function, in agreement with clinical observations *(52)*. The use of CyTOF was instrumental in the analysis of the diversity of leukocytes infiltrating the tumors and allowed simultaneous detection of all major human immune cell subsets, a goal that would not have been possible using classical flow cytometry or histology given the paucity of human cells in the tumor. The spatial localization of the extended diversity of human subsets found in the tumor remains a matter for future studies.

To our knowledge, our study represents the first demonstration that ICOS represents a target to affect human Treg *in vivo* and impact tumor growth, although the direct causality was not established here. The presence of $ICOS^+$ Treg has been described in various cancers, including breast *(25)*, ovarian *(53)*, and gastric *(54)* cancers, melanomas *(55, 56)* and more recently follicular lymphomas *(57)*, suggesting that ICOS-based cancer immunotherapy might be widely applicable.

Methods

Mice and humanization

NOD.SCID.gc-null mice (stock ≠005557) were originally purchased from the Jackson Laboratory and were bred in our own animal facility under a 14hrs-10hrs light cycle with ad libitum food and water. Mice were given Baytril in their water every other week. Newborns NSG mice were reconstituted by intrahepatic injection of 5. 10^4 to 10^5 magnetically-purified $CD34^+$ cord blood cells according to the manufacturer's instructions (Miltenyi, Paris, France) or were purchased from ABCell Bio (Paris, France). Reconstitution was followed over time in the blood by multicolor flow cytometry using the following markers in various combinations of fluorescent dyes: mCD45, hCD45, hCD3, hCD20, hCD4, and hCD8. Validated males and females humanized mice of 16 to 20 weeks old were grafted s.c in the right flank with $1.5.10^6$ MDA-MB-231 breast cancer cells. Mice were euthanized when the tumor reached 3000 mm3 in control groups or 4 to 5 weeks after tumor implantation. All protocols were approved by the French National Ethical Committee on Animal Experimentation (Ce5/2012/025). To assess the effects of the various treatments on tumor growth, a total of 4 experiments are presented. Not every experiment included all conditions. Males and females NSG were randomly dispatched into the various experimental groups to avoid sex-linked effects. Experimental groups were dispatched in different cages to avoid cage-related effects. Tumor growth was monitored in a blinded fashion. The number of mice used in each condition is indicated in the figure legend.

Cell line

The triple-negative ($PR^{neg}ER^{neg}HER\text{-}2^{neg}$) MDA-MB-231 cell line was grown in DMEM media supplemented with 10% FCS, L-glutamine and antibiotics (P/S) (all from Thermo) in tissue culture flasks. Cells were transduced with a lentiviral vector co-expressing GFP and Luciferase to follow efficient engraftment *in vivo* using luciferase and to allow exclusion of tumor cells from the analysis based on GFP expression. Cells were confirmed of being mycoplasma-free by a standard Hoechst-dye coloration on indicator Vero cells before injection into mice. A genetic profiling was established and confirmed the identity of the cell line (Eurofins Forensic Department, Ebersberg, Germany).

Reagents preparation and injection

The 314.8 mAb (mouse IgG1 anti-human ICOS) has been described before *(26)*. Isotype control (mouse IgG1, MOPC-1 clone) was purchased from BioXcell (West Lebanon, NH, USA). For all experiments, 314.8 mAb was diluted in PBS before injection. The MT807R1 recombinant Ig consisting of rhesus IgG1k constant regions and CDRs derived from the anti-human CD8 antibody M-T807 grafted into rhesus variable framework regions. And was provided by the Nonhuman Primate Reagent Resource (NIH contract HHSN272200900037C and grant RR016001) The antibody was expressed *in vitro* using serum free medium and purified by protein-A affinity chromatography. Endotoxin was <1EU/mg. Cyclophosphamide (CTX, Sigma Aldrich) was prepared extemporaneously according to supplier technical data sheet, i.e to 20 mg/ml of injectable water. All reagents were injected intraperitoneally.

Phenotypic analysis of leukocytes in the spleens and tumors of humanized mice

Tumor-draining lymph nodes are absent in NSG mice owing to the lack of the common γc-chain necessary for lymph node organogenesis *(58)*. Splenocytes and tumors were digested with 1.6 mg/ml of collagenase IV and 10 µg/ml of DNAse I (Sigma Aldrich) for 2 hrs at 37° with regular flushing of the tissue. Cells were passed through a 40µm-cell strainer and resuspended in PBS 3% SVF. To eliminate dead cells and debris, tumor cell suspensions were isolated on a Ficoll gradient. Rings were collected, washed and cell pellets were resuspended in PBS 3%SVF before counting with Trypan blue exclusion. Subsequently, 3 to 6. 10^6 cells live cells were stained with corresponding antibodies (lanthanide labeled mAbs for CyTOF or fluorochrome-labeled mAbs for FACS analysis). The details of each panel (each one corresponding to one experiment) can be found in Table S1. For CyTOF, 1 to 3µl of each lanthanide-labelled mAbs was added in 1.5 ml Eppendorf tubes in a final volume of 50µl of Max Par Staining Buffer (Fluidigm, San Francisco, USA), according to manufacturer protocol. Intracellular staining was performed with FOXP3 staining kit (eBioscience, Courtaboeuf, France). Cell events were acquired on the CyTOF-2 mass cytometer and CyTOF software version 6.0.626 (Fluidigm) at the “Plateforme de Cytométrie de la Pitié-Salpétrière (CyPS).” Dual count calibration, noise reduction, cell length threshold between 10 and 150 pushes, and a lower convolution threshold equal to 10 were applied during acquisition. Data files produced by the CyTOF-2 were normalized with the

MatLab Compiler software normalizer using the signal from the 4-Element EQ beads (Fluidigm) as recommended by the software developers. Except for the analysis shown in Fig. 1, GFP exclusion was performed to remove tumor cells from the analysis.

Clinical samples

The main clinical characteristics of the patients are summarized in Table 1. Luminal breast tumors were collected from 7 untreated cancer patients undergoing standard surgery at Institut Curie Hospital, in accordance with institutional ethical guidelines and approved by the ethical (CPP ref: 99-15) and medical (ANSM ref: 2015-A00824-45) committees. Flow cytometry data in those patients were collected prior the initiation of the HuMice study, hence no CyTOF data were collected from human patients.

Tumor samples from patients and cell isolation

Samples were cut into small fragments, digested with 0.1 mg/ml Liberase TL in the presence of 0.1 mg/ml DNase (Roche, Meylan, France) and incubated for 30 min at 37°C in 5% of CO2 incubator. Subsequently, cells were filtered on a 40-µm cell strainer (BD Biosciences, Le Pont-de-Claix, France), washed and submitted to staining with specific antibodies. Peripheral blood from breast cancer patients was collected in tubes containing EDTA, washed in PBS and submitted to staining with specific fluorescent-labelled antibodies.

Phenotypic analysis of leukocytes in whole blood and tumors in human breast cancer patients

Tumor cell suspension and whole blood were stained with LIVE/DEAD Fixable Aqua (Life Technologies, Courtaboeuf, France) for 10 min at RT. Then, cells were washed and stained with Aqua BV500 dead cells exclusion dye (Life Technologies); anti-CD3 (clone OKT3, BV650), anti-CD4 (clone OKT4, BV785), anti-PD-1 (EH122.2H7, BV711), anti-CD27 (O323, BV605) from Biolegend (London, UK); anti-CD45 (clone 2D1, APC Cy7), anti-CD8 (clone RPA-T8, BUV395), anti-CD19 (clone HIB 19, Alexa 700) anti-CD56 (NCAM16.2, BUV737), anti-HLA-DR (G46.6, PECy5), anti-PD-L1 (MIHI, PE-CF594) from BD Biosciences; anti-EpCAM (1B7, eFluor660), anti-CD14 (2G5, FITC), anti-

CD45RA (HI100, PECy7), and anti-ICOS (ISA3, PERCPe710) from eBioscience for 20 min at 4°C. After incubation, cells were washed and permeabilized for 16 hours according to manufacturer's instructions for staining with anti-FOXP3 (236A/E7, PE, eBioscience) and anti-Granzyme-B (GB11, BV421, BD Biosciences). Cells were then fixed for subsequent analysis on a Fortessa flow cytometer (BD Biosciences). Data were analyzed with FlowJo Version v10 (FlowJO LCC, Ashland, USA), or Cytobank (www.cytobank.org).

Mass cytometry data analysis

For CyTOF data analysis, 10 healthy cord blood donors were used in 4 independent experiments, each experiment including mice reconstituted with different donors. A total of 15 mice were analyzed at the steady state by mass cytometry for human and murine cell content in the spleen and the tumor. Due to the paucity of cells in tissues of some HuMice, and to increase resolution of the analysis, tissue samples from 2 to 3 of those mice were pooled before staining and CyTOF analysis. The frequency of $hCD45^+$ determined by flow cytometry was used to normalize the representation of each mouse within the pool. In case where sufficient number of cells were collected, tissue samples from individual mice were run into CyTOF. To normalize the analysis from these various conditions, concatenation of individual mice from the same tissue in the same experiment was performed using FlowJo v10. Therefore, this analysis method does not allow comparisons of individual mice but of individual experiments. To document reproducibility of our observations, we provide frequencies of cells in each of the 4 individual experiments, when applicable. Concatenated samples were exported in Cytobank for unsupervised viSNE analysis or were analyzed using FlowJo v10 for supervised analysis. viSNE is a Cytobank implementation of the t-SNE algorithm originally developed by Amir et al *(21)*. The following settings were applied: 1000 iterations, perplexity of 30 and a theta factor of 0.5.

Statistical analysis

Statistical analyses were performed using Prism v6.0h for Mac (GraphPad) with statistical models indicated in the figure legends. Outliers detection method is reported in the figure legends when applicable. All tests were performed with an α at 0.05 (probability of detecting a difference in the means by chance below 5%). No a priori sample size estimation to fit statistical power with the

observed effect on tumor growth was used. However, a reverse analysis of our data using G-Power for Mac *(59)* showed that given the number of mice used, the observed difference in the means at the end of the experiment and the standard deviations in both groups, the β power (probability of missing a difference in the means below 5%) was >95%.

Author's contributions (CRediT taxonomy *(60)*): Conceptualization, AB, CC, and GM; Methodology, AB and GM; Formal Analysis, AB, RR, KS, AC and GM; Investigation, AB, RR, KS and AC; Resources, EP, DO and CMC; Writing-Original Draft, AB and GM; Writing-Review and editing, AB, RR, EP, CMC, CC and GM; Visualization, GM; Supervision, GM; Funding acquisition, CMC, CC, DO and GM.

Acknowledgements: the authors would like to thank Ms S Just-Landi (Institut Paoli-Calmettes, Marseille, France) for providing the 314.8 mAb, Dr H. Yssel (CIMI-PARIS, Paris, France) for monitoring mycoplasma infection in cell culture, Dr V. Vieillard (CIMI-PARIS) for advice on NK cells analysis, Dr M. Miyara (CIMI-PARIS) and Dr C. Combadière (CIMI-PARIS) for access to Cytobank, Dr B Salomon (CIMI-PARIS) for critical reading of the manuscript, C. Enond, O. Brégerie and B. Kane (Centre d'Exploration Fonctionnelle, Pitié Salpêtrière, Paris, France) for animal husbandry, and all the mothers for cord blood donations and patients for samples. **Funding:** This study was supported by the Ligue Nationale contre le cancer (LNC), the Agence Nationale de la Recherche (ANR-11-EMMA-0045 VICIT) and Glaxo Smith Kline (GSK). Dr A. Burlion was supported by a doctoral fellowship from the French Ministère de l'Education Supérieure et de la Recherche and from LNC. Dr K. Sendeyo was supported by a research contract with GSK. **Competing interests:** The authors declare no competing interests. GSK had neither implication in the design of the experiments nor in the interpretation of the results.

References

1. Wolchok JD et al. Nivolumab plus ipilimumab in advanced melanoma. [Internet]. *N. Engl. J. Med.* 2013;369(2):122–33.

2. Mahoney KM, Rennert PD, Freeman GJ. Combination cancer immunotherapy and new immunomodulatory targets [Internet]. *Nat. Rev. Drug Discov.* 2015;14(8):561–584.

3. Moynihan KD et al. Eradication of large established tumors in mice by combination immunotherapy that engages innate and adaptive immune responses. [Internet]. *Nat. Med.* 2016;22(12):1402–1410.

4. DeRose YS et al. Tumor grafts derived from women with breast cancer authentically reflect tumor pathology, growth, metastasis and disease outcomes. [Internet]. *Nat. Med.* 2011;17(11):1514–20.

5. Valdez KE et al. Human primary ductal carcinoma in situ (DCIS) subtype-specific pathology is preserved in a mouse intraductal (MIND) xenograft model [Internet]. *J. Pathol.* 2011;225(4):565–573.

6. Bankert RB et al. Humanized mouse model of ovarian cancer recapitulates patient solid tumor progression, ascites formation, and metastasis [Internet]. *PLoS One* 2011;6(9):e24420.

7. Quintana E et al. Human melanoma metastasis in NSG mice correlates with clinical outcome in patients. [Internet]. *Sci. Transl. Med.* 2012;4(159):159ra149.

8. Morton JJ, Bird G, Refaeli Y, Jimeno A. Humanized Mouse Xenograft Models: Narrowing the Tumor-Microenvironment Gap. [Internet]. *Cancer Res.* 2016;76(21):6153–6158.

9. Sanmamed MF et al. Nivolumab and Urelumab Enhance Antitumor Activity of Human T Lymphocytes Engrafted in Rag2-/-IL2R null Immunodeficient Mice [Internet]. *Cancer Res.* 2015;75(17):3466–3478.

10. Shultz LD et al. Human Lymphoid and Myeloid Cell Development in NOD/LtSz-scid IL2R null Mice Engrafted with Mobilized Human Hemopoietic Stem Cells [Internet]. *J. Immunol.* 2005;174(10):6477–6489.

11. Marodon G et al. High diversity of the immune repertoire in humanized NOD.SCID.gamma c-/- mice. [Internet]. *Eur. J. Immunol.* 2009;39(8):2136–45.

12. Wege AK et al. Humanized tumor mice-A new model to study and manipulate the immune response in advanced cancer therapy [Internet]. *Int. J. Cancer* 2011;129(9):2194–2206.

13. Escobar G et al. Genetic engineering of hematopoiesis for targeted IFN-α delivery inhibits breast cancer progression. [Internet]. *Sci. Transl. Med.* 2014;6(217):217ra3.

14. Rongvaux A et al. Development and function of human innate immune cells in a humanized mouse model. [Internet]. *Nat. Biotechnol.* 2014;32:364–72.

15. Morton JJ et al. XactMice: humanizing mouse bone marrow enables microenvironment reconstitution in a patient-derived xenograft model of head and neck cancer. [Internet]. *Oncogene* 2016;35(3):290–300.

16. Mahne A et al. Dual roles for regulatory T cell depletion and co-stimulatory signaling in agonistic GITR targeting for tumor immunotherapy. [Internet]. *Cancer Res.* 2016;77(5):1108–1118.

17. Waldron-Lynch F et al. Teplizumab Induces Human Gut-Tropic Regulatory Cells in Humanized Mice and Patients [Internet]. *Sci. Transl. Med.* 2012;4(118):118ra12.

18. Vudattu NK et al. Humanized Mice as a Model for Aberrant Responses in Human T Cell Immunotherapy [Internet]. *J Immunol* 2014;193(2):587–596.

19. Spitzer MH, Nolan GP. Mass Cytometry: Single Cells, Many Features. [Internet]. *Cell* 2016;165(4):780–91.

20. Tanaka A, Sakaguchi S. Regulatory T cells in cancer immunotherapy [Internet]. *Cell Res.* 2017;27(1):109–118.

21. Amir ED et al. viSNE enables visualization of high dimensional single-cell data and reveals phenotypic heterogeneity of leukemia. [Internet]. *Nat. Biotechnol.* 2013;31(6):545–52.

22. See P et al. Mapping the human DC lineage through the integration of high-dimensional techniques. [Internet]. *Science* 2017;356(6342):eaag3009.

23. Miyara M et al. Functional Delineation and Differentiation Dynamics of Human CD4+ T Cells Expressing the FoxP3 Transcription Factor [Internet]. *Immunity* 2009;30(6):899–911.

24. Ito T et al. Two functional subsets of FOXP3+ regulatory T cells in human thymus and periphery [Internet]. *Immunity* 2008;28(6):870–880.

25. Gobert M et al. Regulatory T Cells Recruited through CCL22/CCR4 Are Selectively Activated in Lymphoid Infiltrates Surrounding Primary Breast Tumors and Lead to an Adverse Clinical Outcome [Internet]. *Cancer Res.* 2009;69(5):2000–2009.

26. Faget J et al. ICOS-ligand expression on plasmacytoid dendritic cells supports breast cancer progression by promoting the accumulation of immunosuppressive CD4+ T cells. [Internet]. *Cancer Res.* 2012;72(23):6130–41.

27. Faget J et al. ICOS is associated with poor prognosis in breast cancer as it promotes the amplification of immunosuppressive CD4(+) T cells by plasmacytoid dendritic cells. [Internet]. *Oncoimmunology* 2013;2(3):e23185.

28. Pfirschke C et al. Immunogenic Chemotherapy Sensitizes Tumors to Checkpoint Blockade Therapy [Internet]. *Immunity* 2016;44(2):343–354.

29. Sistigu A et al. Immunomodulatory effects of cyclophosphamide and implementations for vaccine design. *Semin. Immunopathol.* 2011;1–15.

30. Schmitz JE et al. A nonhuman primate model for the selective elimination of CD8+ lymphocytes using a mouse-human chimeric monoclonal antibody [Internet]. *Am J Pathol* 1999;154(6):1923–1932.

31. Petit NY, Lambert-Niclot S, Marcelin A-G, Garcia S, Marodon G. HIV Replication Is Not Controlled by CD8+ T Cells during the Acute Phase of the Infection in Humanized Mice. [Internet]. *PLoS One* 2015;10(9):e0138420.

32. Stanton SE, Disis ML. Clinical significance of tumor-infiltrating lymphocytes in breast cancer. [Internet]. *J. Immunother. cancer* 2016;4(2):59.

33. Stanton SE, Adams S, Disis ML. Variation in the Incidence and Magnitude of Tumor-Infiltrating Lymphocytes in Breast Cancer Subtypes A Systematic Review. *JAMA Oncol* 2016;2(10):1354–1360.

34. Gajewski TF, Schreiber H, Fu Y-X. Innate and adaptive immune cells in the tumor microenvironment [Internet]. *Nat. Immunol.* 2013;14(10):1014–1022.

35. Dong C et al. ICOS co-stimulatory receptor is essential for T-cell activation and function. [Internet]. *Nature* 2001;409(6816):97–101.

36. Hutloff A et al. ICOS is an inducible T-cell co-stimulator structurally and functionally related to CD28.. *Nature* 1999;397(6716):263–266.

37. Tafuri A et al. ICOS is essential for effective T-helper-cell responses [Internet]. *Nature* 2001;409(6816):105–109.

38. Wikenheiser DJ, Stumhofer JS. ICOS Co-Stimulation: Friend or Foe? [Internet]. *Front. Immunol.* 2016;7(AUG):304.

39. Tuettenberg A et al. The Role of ICOS in Directing T Cell Responses: ICOS-Dependent Induction of T Cell Anergy by Tolerogenic Dendritic Cells [Internet]. *J. Immunol.* 2009;182(6):3349–3356.

40. Bulliard Y et al. Activating Fc γ receptors contribute to the antitumor activities of immunoregulatory receptor-targeting antibodies. [Internet]. *J. Exp. Med.* 2013;210(9):1685–1693.

41. Simpson TR et al. Fc-dependent depletion of tumor-infiltrating regulatory T cells co-defines the efficacy of anti-CTLA-4 therapy against melanoma. [Internet]. *J. Exp. Med.* 2013;210(9):1695–710.

42. Selby MJ et al. Anti-CTLA-4 Antibodies of IgG2a Isotype Enhance Antitumor Activity through Reduction of Intratumoral Regulatory T Cells [Internet]. *Cancer Immunol. Res.* 2013;1(1):32–42.

43. Bulliard Y et al. OX40 engagement depletes intratumoral Tregs via activating FcγRs, leading to antitumor efficacy. [Internet]. *Immunol. Cell Biol.* 2014;92(6):475–80.

44. Romano E et al. Ipilimumab-dependent cell-mediated cytotoxicity of regulatory T cells ex vivo by nonclassical monocytes in melanoma patients [Internet]. *Proc. Natl. Acad. Sci.* 2015;112(19):201417320.

45. Chang D-K et al. Anti-CCR4 monoclonal antibody enhances antitumor immunity by modulating tumor-infiltrating Tregs in an ovarian cancer xenograft humanized mouse model. [Internet]. *Oncoimmunology* 2016;5(3):e1090075.

46. Marabelle A et al. Depleting tumor-specific Tregs at a single site eradicates disseminated tumors [Internet]. *J. Clin. Invest.* 2013;123(6):2447–2463.

47. Sukumar S et al. Characterization of MK-4166, a clinical agonistic antibody that targets human GITR and inhibits the generation and suppressive effects of T regulatory cells [Internet]. *Cancer Res.* 2017;77(29):canres.1439.2016.

48. Plitas G et al. Regulatory T Cells Exhibit Distinct Features in Human Breast Cancer [Internet]. *Immunity* 2016;45(5):1122–1134.

49. Metzger TC et al. ICOS promotes the function of CD4+ effector T cells during anti-OX40-mediated tumor rejection [Internet]. *Cancer Res.* 2016;76(13):3684–3689.

50. Broz ML et al. Dissecting the Tumor Myeloid Compartment Reveals Rare Activating Antigen-Presenting Cells Critical for T Cell Immunity [Internet]. *Cancer Cell* 2014;26(5):638–652.

51. Gabrilovich DI, Ostrand-Rosenberg S, Bronte V. Coordinated regulation of myeloid cells by tumours [Internet]. *Nat Rev Immunol* 2012;12(4):253–268.

52. Mamessier E et al. Human breast cancer cells enhance self tolerance by promoting evasion from NK cell antitumor immunity. [Internet]. *J. Clin. Invest.* 2011;121(9):3609–22.

53. Conrad C et al. Plasmacytoid dendritic cells promote immunosuppression in ovarian cancer via ICOS costimulation of Foxp3+ T-regulatory cells. *Cancer Res.* 2012;72(20):5240–5249.

54. Nagase H et al. ICOS $^{+}$ Foxp3 $^{+}$ TILs in gastric cancer are prognostic markers and effector regulatory T cells associated with *H elicobacter pylori* [Internet]. *Int. J. Cancer* 2016;1–10.

55. Martin-Orozco N et al. Melanoma cells express ICOS ligand to promote the activation and expansion of T-regulatory cells. [Internet]. *Cancer Res.* 2010;70(23):9581–90.

56. Strauss L et al. Expression of ICOS on human melanoma-infiltrating CD4+CD25highFoxp3+ T regulatory cells: implications and impact on tumor-mediated immune suppression. [Internet]. *J. Immunol.* 2008;180(5):2967–80.

57. Le K-S et al. Follicular B Lymphomas Generate Regulatory T Cells via the ICOS/ICOSL Pathway and Are Susceptible to Treatment by Anti-ICOS/ICOSL Therapy. [Internet]. *Cancer Res.* 2016;76(16):4648–60.

58. Mebius RE. Organogenesis of lymphoid tissues [Internet]. *Nat Rev Immunol* 2003;3(4):292–303.

59. Faul F, Erdfelder E, Lang AG, Buchner A. G* Power 3: A flexible statistical power analysis program for the social, behavioral, and biomedical sciences. *Behav. Res. Methods* 2007;39(2):175–191.

60. Brand A, Allen L, Altman M, Hlava M, Scott J. Beyond authorship: Attribution, contribution, collaboration, and credit. *Learn. Publ.* 2015;28(2):151–155.

Cod. Pat.	Age (years)	Meno status	Histo.	Grad.	Size (mm)	pTNM	ER (%)	PR (%)	HER2 status	Ki67 (%)	TIL (%)
808220	86	yes	Lobular	2	21	pT2N3M0	100	0	neg	20	15
808243	55	yes	Ductal	2	30	pT2N1M0	100	15	neg	20	5
808254	65	yes	Ductal	2	25	pT2N2M0	95	95	neg	15	NA
808364	52	yes	Ductal	2	18	pT1N2M0	90	80	neg	15	<10
808430	32	no	Ductal	2	26	pT2N2M0	100	95	neg	40	20
809090	40	no	Ductal	3	25	pT2N2M0	90	90	neg	40	30
809113	60	yes	Ductal	2	28	pT2N1M0	100	30	pos	17	10

Table 1. Clinical characteristics of the primary breast tumors samples. Cod. Pat.= Patient code/ Age= age of the patient at the time of surgery/Meno. status = Menopausal status/ Histo.= Histologic type/ Grade= SBR Grade (histo-prognostic grade based on "Scarff-Bloom-Richardson")/ pTNM= tumor classification based on Tumor-Nodes-Metastasis score/ ER= % of estrogen receptor positivity/ PR= % of progesterone receptor positivity/ Ki67%= cellular marker of proliferation/ TILs=% of Tumor-infiltrated Lymphocytes.

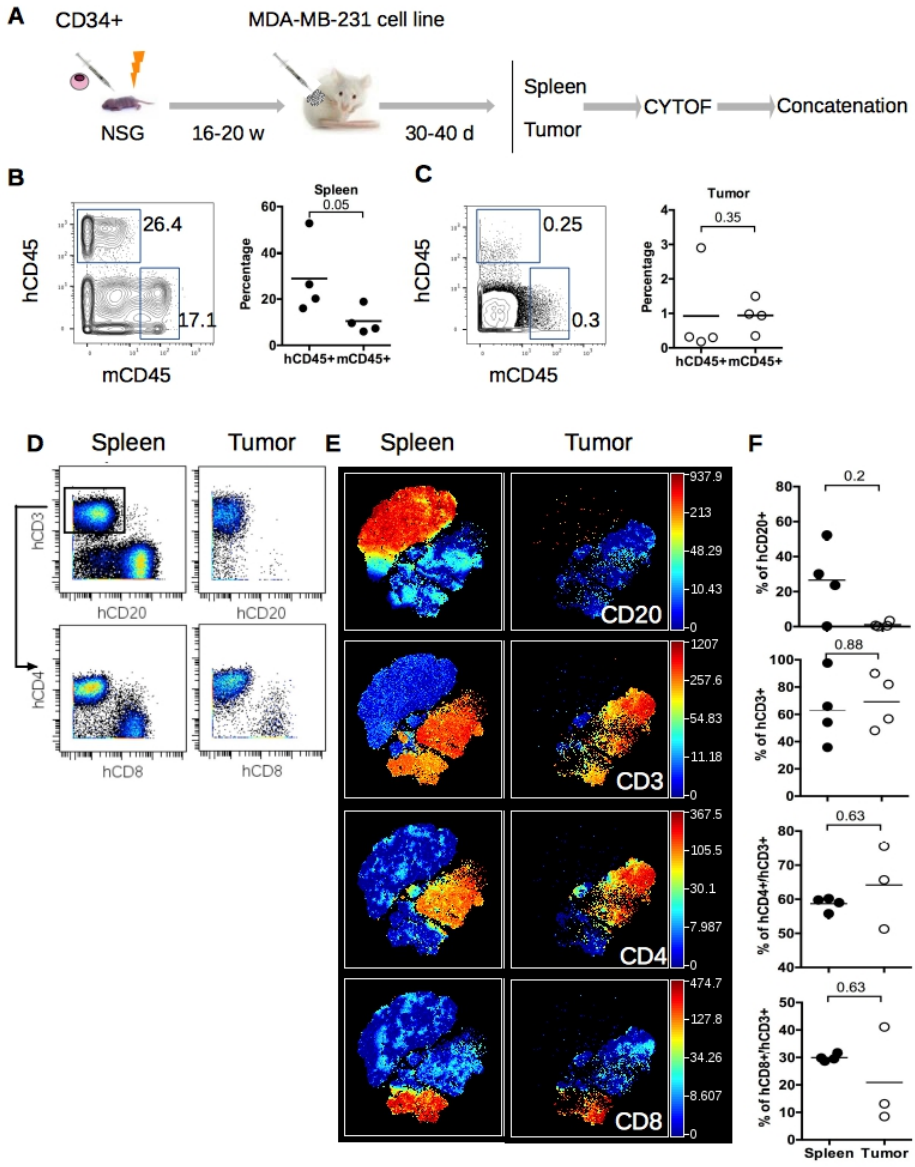

Fig 1. Distribution of human and murine leukocytes in HuMice. (A) Experimental scheme of the study. **(B-C)** Frequencies of human and murine hematopoietic cells in the spleen **(B)** and the tumor **(C)** of HuMice were determined based on hCD45$^+$ and mCD45$^+$ expression as depicted. Each dot is an experiment. Negative cells are split in two on each axes due to the arc sin transformation of CyTOF data and arbitrary settings for best 2D representation in FlowJo. **(D)** Representative profile in the spleen and the tumor of HuMice for the indicated markers. 2D plots were extracted from CyTOF data in a representative experiment. **(E)** viSNE representation of gated human CD45$^+$ cells in the spleen and the tumor from a representative experiment. The viSNE plot was generated according to NKp46, CD38, CD33, CD45RO, PD-1, CD4, CD8, CD20, CD25, Grz-B, and HLA-DR expression using proportional sampling with 54422 events in the spleen and 10274 events in the tumor. The level of expression of each of the indicated markers is represented by a color scale on the right. **(F)** Frequencies of the indicated subsets were determined by supervised 2D-gating from CyTOF data. Each dot represents an experiment. Horizontal line represents the mean value. Four independent experiments totalizing 15 mice were performed. The p-values in B, C and F are from non-parametric two-tailed Mann-Whitney t-test.

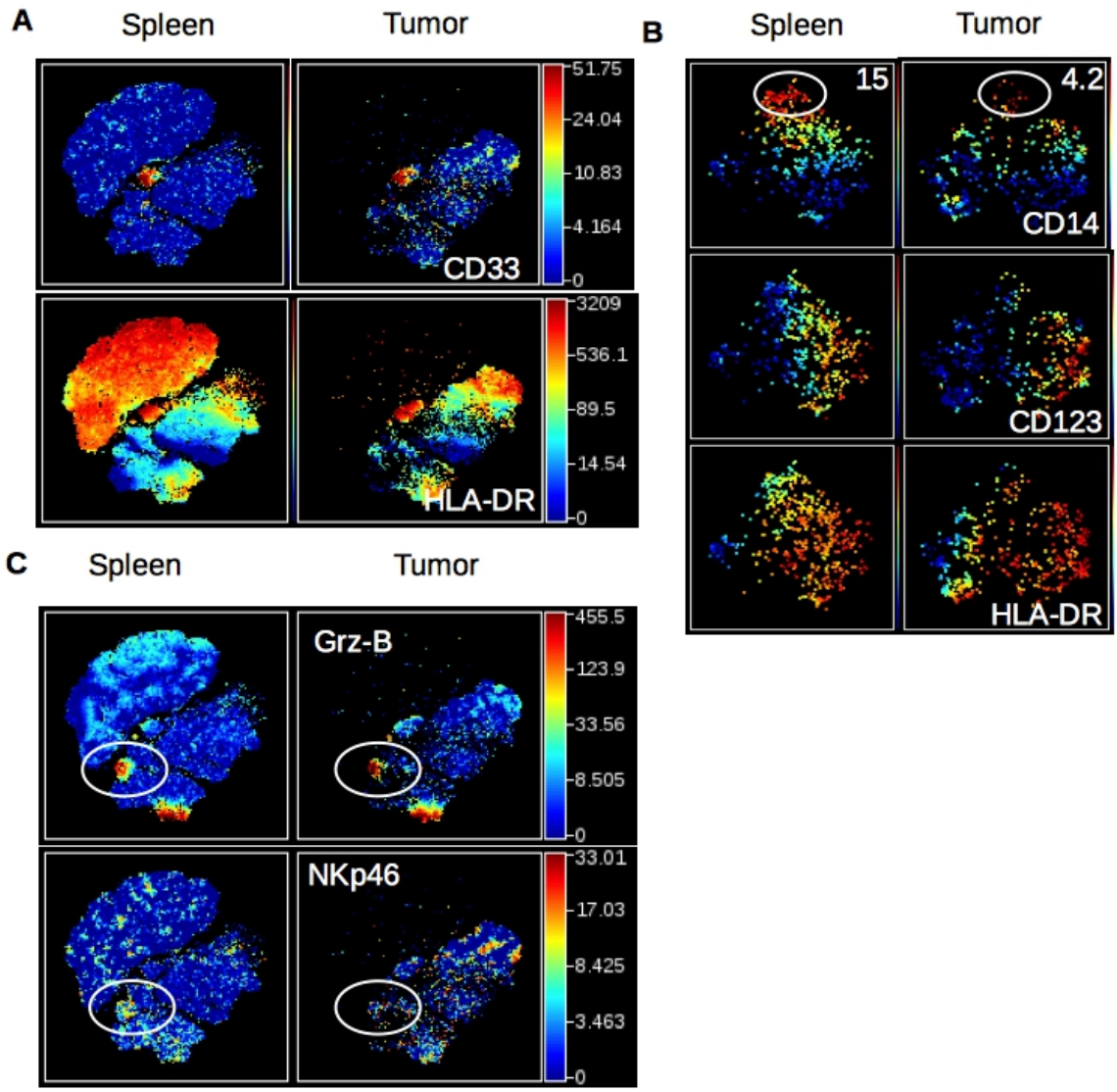

Fig 2. Detection of human myeloid cells and NK cells in HuMice. (A) The viSNE plot was generated as in Fig. 1E and represents the expression of CD33 and HLA-DR in hCD45$^+$ cells of the spleen and tumor. **(B)** The viSNE plots were generated in gated hCD45$^+$CD33$^+$ cells according to CD14, CD45RO, CD123, CD4, CD11b and HLA-DR expression using proportional sampling with 535 cells in the spleen and 476 events in the tumors. Indicated on the plots are the frequencies of CD14-expressing cells in the CD33$^+$ cluster. **(C)** The visNE plots was generated as in Fig. 1E and represents the expression of Granzyme-B (Grz-B) and NKp46 in the spleen and the tumor. Gates highlight the localization of putative NK cells.

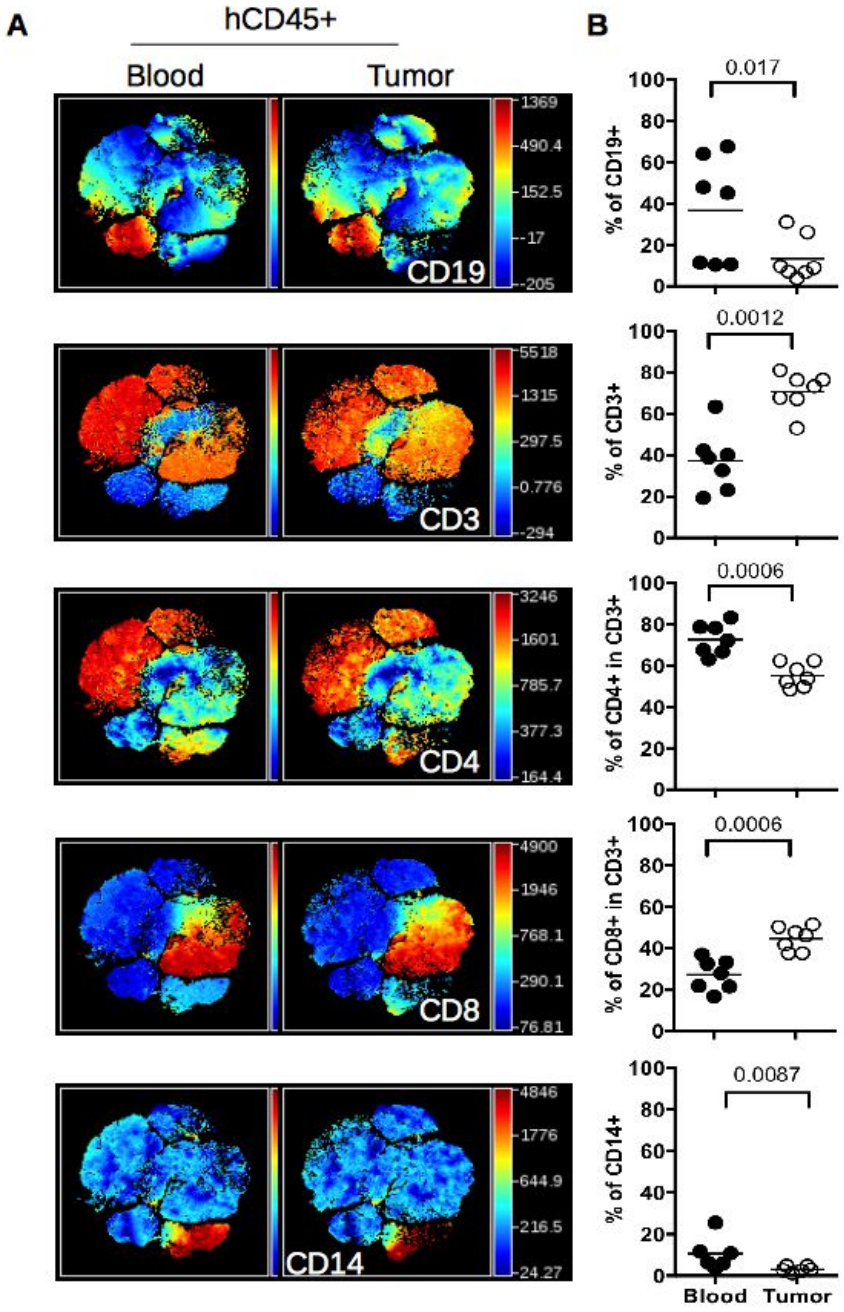

620 **Fig 3. Distribution of human leukocytes in breast cancer patients. (A)** viSNE representation of flow cytometry data in gated human CD45^{+} (hCD45^{+}) cells in the blood and the tumor of a representative breast cancer patient. The viSNE plot was generated according to CD14, HLA-DR, FOXP3, CD19, CD8 and CD4 expression using proportional sampling with 50 000 events in each tissue. The MFI (median fluorescence intensity) of each marker is represented by a color scale on the right. **(B)** 625 Frequencies of the indicated subsets were determined by supervised 2D- analysis. Each dot is a patient. Horizontal line represents the mean value. The p-values reported on the graphs are from a non-parametric two-tailed Mann Whitney t-test.

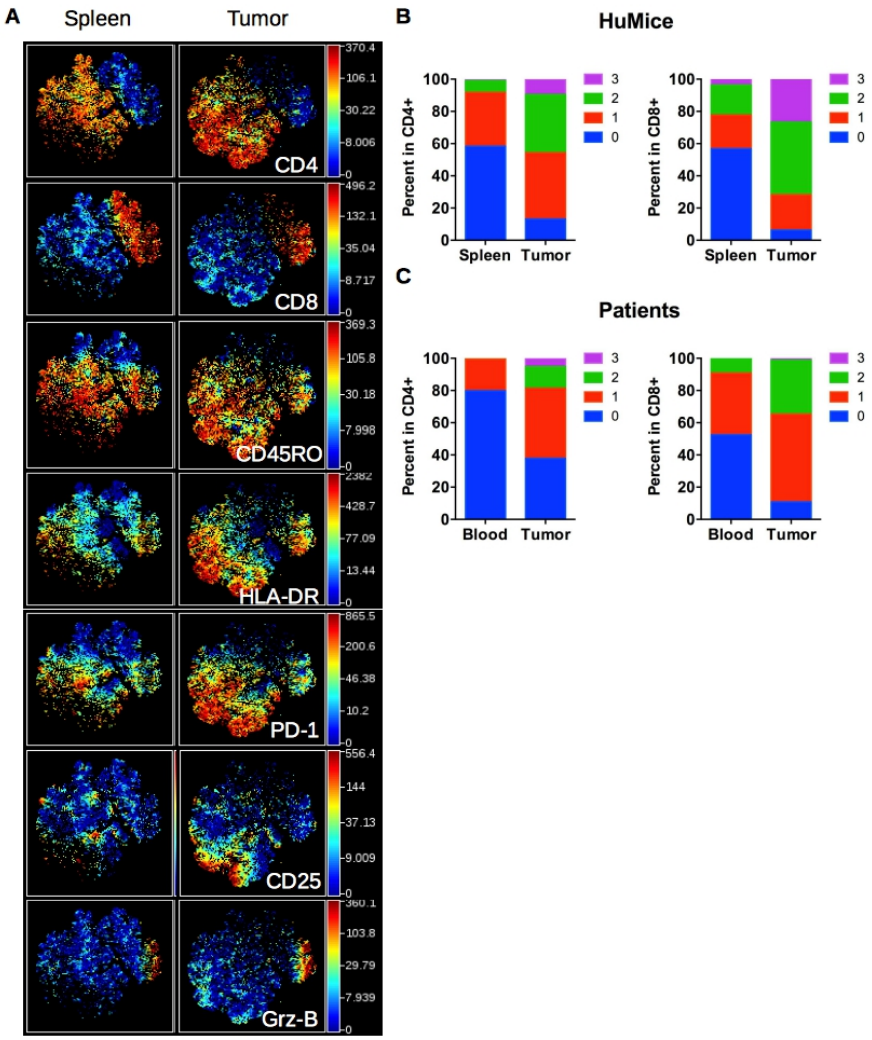

Fig 4. Activation status of Tumor-infiltrating T cells of HuMice and breast cancer patients. (A) hCD45$^+$CD3$^+$ from HuMice were gated in Cytobank and a viSNE plot was generated according to Ki-67, CD45R0, PD-1, CD4, CD8, CD25, Grz-B and HLA-DR expression using equal sampling with 8574 events in the spleen and tumor. **(B)** Frequencies of cells expressing 0, 1, any combination of 2 or all 3 activation markers are shown in the indicated tissue. Activation markers used for boolean analysis were CD25, HLA-DR and PD-1 for CD4$^+$ T cells and HLA-DR, Grz-B and CD45RO for CD8$^+$ T cells. Results are from one experiment out of 3. **(C)** Same analysis for T cells from breast cancer patients. Results are cumulative frequencies in 7 breast cancer patients in 7 independent experiments in the blood and the tumor determined by flow cytometry. The activation markers used for boolean analysis were HLA-DR, ICOS and PD-1 for CD4$^+$ T cells and CD45RA, Grz-B and HLA-DR for CD8$^+$ T cells (negativity for CD45RA was considered as an activated phenotype).

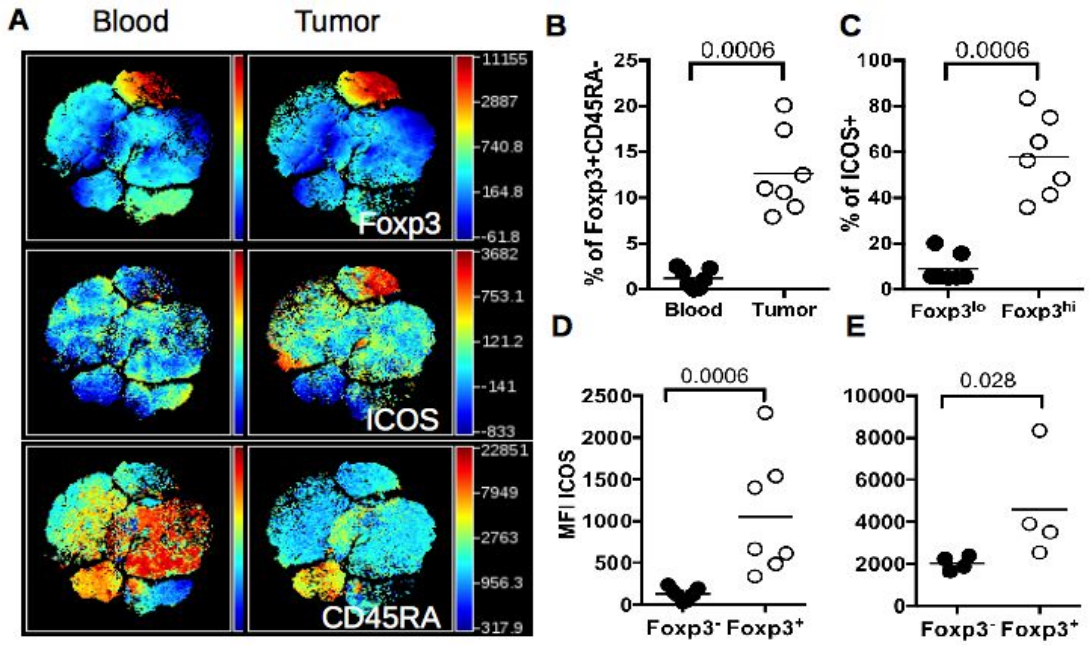

Fig 5. ICOS expression by Treg in HuMice and breast cancer patients. (A) viSNE plot of hCD45^{+} from a representative breast cancer patient showing FOXP3, ICOS and CD45RA expression in the blood and the tumor, determined by flow cytometry. **(B)** Frequencies of FOXP3^{+}CD45RA^{neg} cells in the indicated tissue from breast cancer patients in total CD4^{+}CD3^{+} cells. **(C)** Frequencies of ICOS^{+} cells in FOXP3^{lo} or FOXP3^{hi} CD4^{+}CD45RA^{neg} in the tumor of breast cancer patients. **(D-E)** MFI of ICOS in the indicated subsets in the tumor of breast cancer patients **(D)** or in the tumor of HuMice **(E)** for the indicated subsets. Horizontal line represents the mean value. Data are cumulative of at least 3 independent experiments. Each dot represents a patient or a mouse. The p values indicated on the graphs are from non-parametric two-tailed Mann-Whitney t-test.

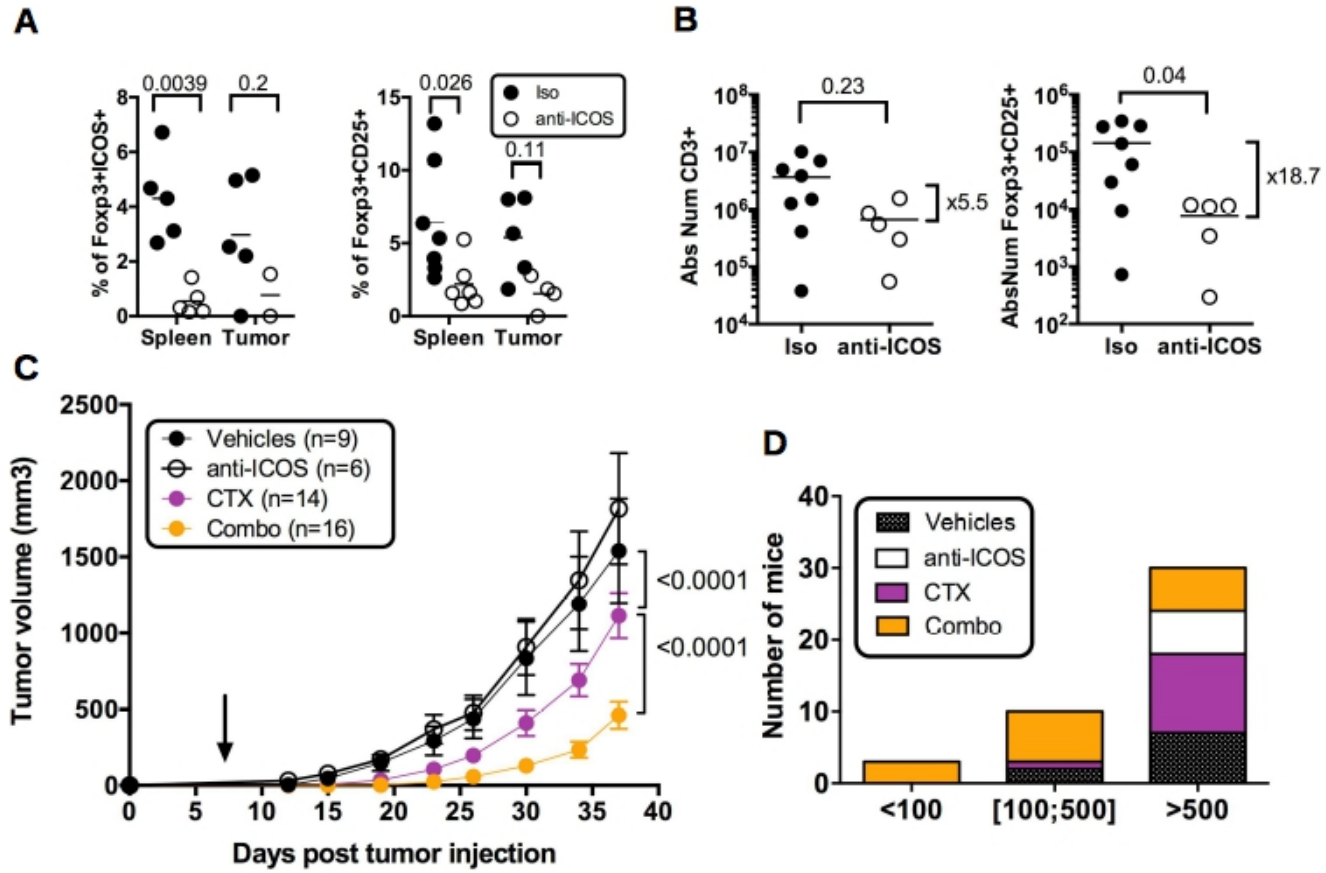

Fig 6. I**mpact of anti-ICOS mAb on Treg and tumor growth in HuMice. (A)** Frequencies of $FOXP3^+ICOS^+$ or $FOXP3^+CD25^+$ cells in $CD4^+CD3^+$ T cells in the spleen and tumor of HuMice injected with isotype control (Iso) or anti-ICOS mAb (50µg/mouse). Results shown are cumulative of at least 3 independent experiments. Only high expressing cells were gated. The p-values reported on the graph are from a 2-way ANOVA with multiple comparisons test corrected by the Sidak method. **(B)** Absolute numbers of total T cells ($CD3^+$) or Treg ($FOXP3^+CD25^+$) were based on absolute counts of the spleen of HuMice treated with isotype control (Iso) or anti-ICOS mAb. Each dot represents a mouse. Fold change in mean numbers are indicated on the right. The p-values indicated on the graphs are from an unpaired two-tailed non-parametric Kolgomorov-Smirnov t-test. Data are cumulative of at least 3 independent experiments. Horizontal line represents the mean value. **(C)** Tumor growth was determined in 4 independent experiments in the indicated number of mice treated by PBS and isotype control (Vehicles), anti-ICOS and PBS (anti-ICOS; 50 µg/mouse), cyclophosphamide and isotype control (CTX; 1.5 mg/mouse) or a combination of CTX and anti-ICOS (Combo). The null hypothesis stating that one curve fits all the data in the compared groups (indicated by brackets on the graph) was rejected based on the low p-value determined by nonlinear regression modeling of the data using the exponential growth equation. Error bars are SEM. **(D)** Number of mice bearing tumor size below 100mm3 (<100), between 100 and 500mm3 ([100;500]) and greater than 500mm3 (>500) is shown for the indicated groups.

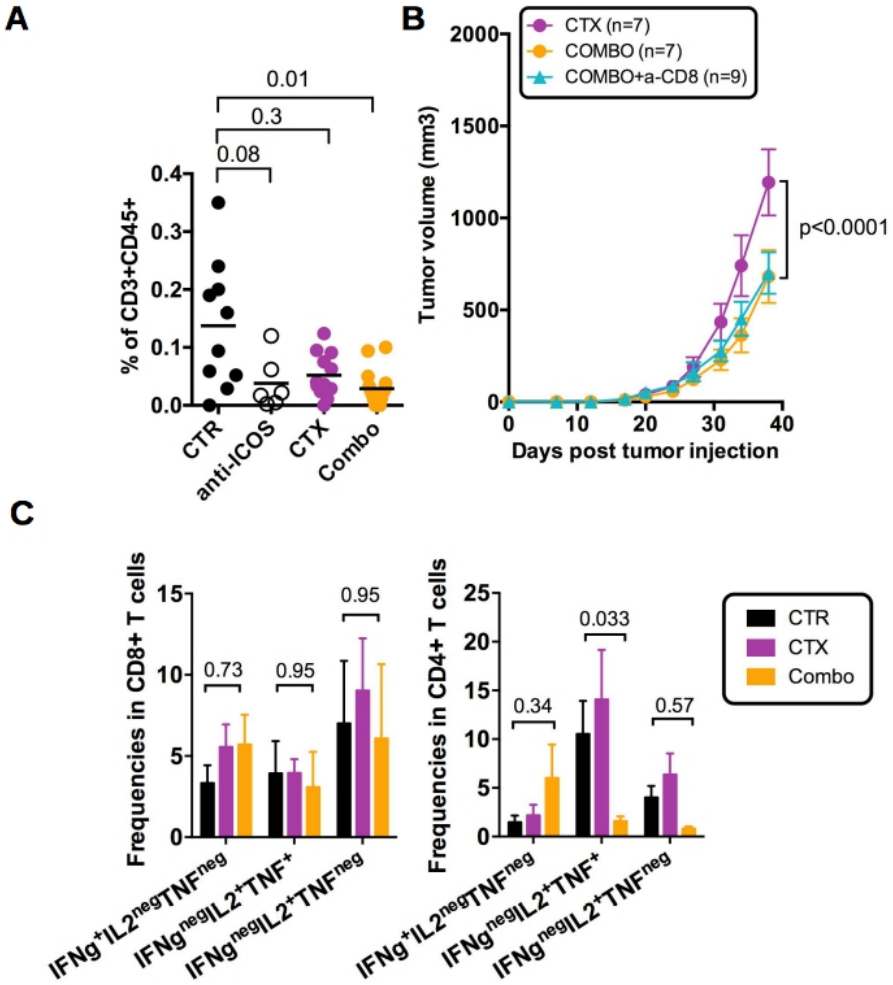

Fig. 7. Role of human T cells in the prevention of tumor growth by the combination of chemotherapy and anti-ICOS mAb. (A) Frequencies of $CD3^+CD45^+$ human T cells in the tumor of the indicated groups. Each dot is a mouse. Results are cumulative from 4 independent experiments. One outlier in the CTX and one in the combo groups were detected by the Rout method (Q=0.5%) and were excluded from the analysis. The p-values indicated on the graphs are from a Kruskall-Wallis test with Dunn's corrections. **(B)** Tumor growth in the absence of $CD8^+$ T cells in the combo group. CD34-reconstituted NSG mice were grafted s.c with the MDA-MB-231 cell line, injected with cyclophosphamide only (CTX; 1.5 mg/mouse) or CTX and the anti-ICOS mAb (50 µg/mouse) with (Combo+a-CD8) or without (Combo) the MT807R1 recombinant Ig (10mg/kg). Results are cumulative of 2 independent experiments (total numbers of mice at the start of the experiment are indicated in brackets). Error bars are SEM. The low p-value indicate the low probability that one curve fits all the data points between CTX and Combo+a-CD8 using a non linear regression exponential growth statistical modeling of the data. **(C)** Frequencies of $CD8^+$ (left panel) and $CD4^+$ (right panel) T cells expressing the combination of the indicated cytokines were determined by flow cytometry in the control (CTR), CTX-only (CTX) or CTX and anti-hICOS mAb (Combo) after 4 hrs of PMA/ionomycine stimulation of total splenocytes. The indicated p-values are from 2-way ANOVA with Dunnet correction for multiple comparisons between the CTR and the Combo group. Results are from a single experiment with 3 mice per group.